Peer Reviewed Paper openaccess Special Issue on Spectral Imaging in Synchrotron Light Facilities

Assessment of adeno-associated virus gene therapies efficacy on acid alpha-glucosidase restoration and glycogen storage correction in cardiac muscle of Pompe disease mice using synchrotron infrared and ultraviolet microspectroscopies

Laurence Dubreil,[a,#,*] Lydie Lagalice,[b,#] Johan Deniaud,[b] Antoine Sabourin,[b] Claire Lovo,[c] Karim Bey,[b] Juliette Hordeaux,[b] Chantal Thorin,[d] Christophe Sandt,[e] Frédéric Jamme[f] and Marie-Anne Colle[g]

[a]PAnTher, INRA, École Nationale Vétérinaire, Agro-alimentaire et de l'alimentation Nantes-Atlantique (Oniris), Nantes, F-44307, France. E-mail: laurence.dubreil@oniris-nantes.fr, https://orcid.org/0000-0002-4892-0426

[b]PAnTher, INRA, École Nationale Vétérinaire, Agro-alimentaire et de l'alimentation Nantes-Atlantique (Oniris), Nantes, F-44307, France

[c]PAnTher, INRA, École Nationale Vétérinaire, Agro-alimentaire et de l'alimentation Nantes-Atlantique (Oniris), Nantes, F-44307, France. https://orcid.org/0000-0002-8014-1676

[d]Laboratoire de Physiopathologie Animale et Pharmacologie Fonctionnelle, Oniris, Nantes, France. https://orcid.org/0000-0002-5688-1834

[e]Synchrotron SOLEIL, L'Orme des Merisiers Saint Aubin, Gif-sur-Yvette, France. https://orcid.org/0000-0002-6432-2004

[f]Synchrotron SOLEIL, L'Orme des Merisiers Saint Aubin, Gif-sur-Yvette, France. https://orcid.org/0000-0002-7398-7868

[g]PAnTher, INRA, École Nationale Vétérinaire, Agro-alimentaire et de l'alimentation Nantes-Atlantique (Oniris), Nantes, F-44307, France. https://orcid.org/0000-0003-3882-7735

[#]Contributed equally

Pompe disease (glycogen storage disease type II) is a lysosomal storage disorder due to a mutation in the gene that encodes acid alpha-glucosidase (GAA). GAA deficiency causes the excessive storage of lysosomal glycogen in many cell types, leading to cell and, subsequently, tissue dysfunction. Cardiac, respiratory and skeletal muscles are the most severely affected. Enzyme replacement therapy (ERT) with recombinant human GAA (rhGAA, Myozyme®, Genzyme, Cambridge) is the only approved treatment for Pompe disease. A new therapeutic strategy was developed consisting of delivering adeno-associated virus serotype 9 (AAV9) and serotype 10 (AAV10) vectors expressing human GAA into cerebrospinal fluid of GAA-KO $6^{neo}/6^{neo}$ Pompe mice. The purpose of this work was to investigate synchrotron Fourier transform infrared (sFT-IR) and deep ultraviolet (sDUV) microspectroscopies to detect new biomarkers of the disease and the AAV gene therapy in the cardiac muscle, one of the most affected organs in Pompe disease. Multivariate statistics applied to sFT-IR spectra between 4000 cm^{-1} and 950 cm^{-1} highlighted the potential of sFT-IR to discriminate Pompe (-/-), Wild type and AAV-treated animals from C–H stretching vibrations of CH_3, from C–O, C–N and C–C stretching vibrations of amide I, II, III bands and from specific IR signature of the glycogen. Investigations performed by sDUV microscopy showed a significant increase

Correspondence
L. Dubreil (laurence.dubreil@oniris-nantes.fr)

Received: 28 February 2019
Revised: 11 June 2019
Accepted: 2 July 2019
Publication: 5 August 2019
doi: 10.1255/jsi.2019.a13
ISSN: 2040-4565

Citation
L. Dubreil, L. Lagalice, J. Deniaud, A. Sabourin, C. Lovo, K. Bey, J. Hordeaux, C. Thorin, C. Sandt, F. Jamme and M.-A. Colle, "Assessment of adeno-associated virus gene therapies efficacy on acid alpha-glucosidase restoration and glycogen storage correction in cardiac muscle of Pompe disease mice using synchrotron infrared and ultraviolet microspectroscopies", *J. Spectral Imaging* **8,** a13 (2019). https://doi.org/10.1255/jsi.2019.a13

of the tryptophan autofluorescent signal in the right ventricle for the AAV9-treated Pompe mice. The high-resolution sDUV microspectroscopy experiments suggested a correlation between the tryptophan-rich area and the GAA-rich area. These unprecedented results demonstrate that high-resolution UV microspectroscopy can be a complementary innovative approach to monitor the chemical change in label-free cardiac muscle section. Moreover, this non-destructive technology can be applied to a small amount of tissue allowing therapeutic assessment from biopsy of human patients.

Keywords: Pompe disease, glycogenosis type II, gene therapy, cardiac muscle, synchrotron microspectroscopy, infrared, glycogen, deep ultraviolet, tryptophan

Introduction

Glycogenosis type II, also known as Pompe disease, is a lysosomal storage disorder caused by mutation in the gene that encodes acid alpha-glucosidase (GAA), which hydrolyses lysosomal glycogen.[1,2] It is an autosomal recessive neuromuscular disorder with an estimated incidence of 1 in 40,000 births.[3–5] GAA deficiency results in lysosomal glycogen storage in multiple tissues that predominantly affects cardiac and skeletal muscles.[2,6] Clinically, infantile-onset Pompe disease manifests as hypotonia, cardiorespiratory distress and cardiomegaly.[7–10] Enzyme replacement therapy (ERT) with recombinant human GAA (rhGAA, Myozyme®, Genzyme, Cambridge) is the only approved treatment for Pompe disease.[11] Treatment with Myozyme® has been shown to increase the patient's lifespan by reducing cardiac pathology,[12,13] however, ERT has a poor and highly variable response in skeletal muscle.[14–17] It was demonstrated that glycogen accumulation also occurs in the central nervous system (CNS)[6,18] and cannot be corrected by ERT due to the blood brain barrier. Patients harbouring the infantile form treated using Myozyme® ERT displayed an extension of life survival, however, they could develop a new neurologic phenotype.[19–21] The requirement of frequent infusions with high concentrations of rhGAA to achieve efficacy and the risk of a subsequent immune response are other drawbacks of ERT treatment in Pompe disease.[22,23] Therefore, development of alternative therapeutic strategies that would efficiently correct the CNS glycogen overload as well as other tissues, such as gene therapy are needed. We previously demonstrated that a single administration of an adeno-associated virus serotype 9 and 10 (AAV9 and AAVrh10) expressing green fluorescent protein transgene (GFP) into the cerebrospinal fluid (CSF) leads to widespread GFP distribution into the brain, spinal cord and peripheral organs in rodent models.[24,25] We also demonstrated that intra-CSF administration of an AAV9 and AAVrh10 expressing hGAA therapeutic transgene in GAA-KO $6^{neo}/6^{neo}$ Pompe mice, allowed significant decrease of glycogen storage into the brain, spinal cord and cardiac muscle, at the histological and molecular levels, with higher efficiency using serotype 9.[26] Significant functional neurologic correction was obtained starting at four months and hypertrophic cardiomyopathy correction was observed at twelve months in AAV9-treated animals. Classical methods for histologic investigation of glycogen storage are based on periodic acid Schiff (PAS) staining in Pompe disease patients as well as in animal models.[27–30] Despite the fact that PAS staining represents the gold standard method for diagnosis in patients and for biomarkers in research, it remains a semi-quantitative method that could, therefore, lead to bias. Recently, Lagalice *et al.*[31] have shown that Fourier transform infrared (FT-IR) microspectroscopy could be an alternative method to characterise glycogen mapping in skeletal muscle from Pompe mice. This non-destructive method based on the vibrational analyses of glycogen represented an unbiased method useful to follow the course of the disease in skeletal muscle.[31]

The purpose of the present study was to assess cardiac muscle correction after hGAA-AAV gene therapy in GAA-KO $6^{neo}/6^{neo}$ Pompe mice using synchrotron radiation as a new tool. FT-IR microscopy coupled to a synchrotron source (sFT-IR) allows both high spatial resolution and high signal-to-noise ratio to be achieved, offering a highly sensitive signal detection of chemical modifications at the cellular level without staining.[32] In addition, synchrotron deep ultraviolet (sDUV) fluorescence microscopy and microspectroscopy are powerful tools to investigate the autofluorescent components of cells and tissues.[33–35] Nicotinamide adenine dinucleotide (NADH), collagen cross-links, tyrosine, elastin and tryptophan can

be localised without any external probe or staining at high spatial resolution.[35–40]

In this study, we highlight the potential of sFT-IR microspectroscopy to investigate the cardiac muscle during the course of Pompe disease as well as to assess the efficacy of hGAA-AAV vectors in GAA-KO $6^{neo}/6^{neo}$ mice. Multivariate statistics applied to IR spectra between 4000 cm^{-1} and 950 cm^{-1} highlighted the potential of sFT-IR to discriminate Pompe, Wild type (Wt) and AAV-treated animals from C–H stretching vibrations of CH_3 and CH_2 (3000–2800 cm^{-1}), from C–O, C–N and C–C stretching vibrations of amide I, II, III bands (1700–1300 cm^{-1}) and from specific IR signatures of glycogen (1152 cm^{-1}, 1080 cm^{-1}, 1025 cm^{-1}).

On the other hand, investigations performed on heart by sDUV showed a significant increase of the tryptophan autofluorescent signal in the right ventricle for the AAV9-treated Pompe mice. High-resolution UV microspectroscopy experiments suggested a correlation between the tryptophan-rich area and the GAA-rich area, detected in parallel by immunohistochemistry in serial thin-sections. These unprecedented results propose complementary highly resolved and sensitive approaches to assess therapeutic strategies in cardiac muscle by monitoring chemical changes. This technology that can be applied to a small amount of tissue is relevant and useful for biopsies from human patients.

Methods

Biological material

Production of vectors

The recombinant viral vectors AAV9-CAG-rhGAA and AAV10-CAG-rhGAA used for gene therapy were produced by the Vector Production Center of the INSERM U1089 unit in Nantes, France. The gene of interest is that encoding human GAA.

Animals and cross-sections preparation

The studies were performed in a Pompe disease mice model (GAA-KO $6^{neo}/6^{neo}$; Nina Raben, NIH, Bethesda, MD, USA). Experiments on animals were carried out according to European guidelines for the care and use of experimental animals, and were reviewed and approved by the regional ethics committee (CEEA Pays de la Loire, authorisation number CEEA-2012-210). IR microspectroscopy studies were first performed on three Wt mice and three GAA-KO $6^{neo}/6^{neo}$ mice, one-month old and twelve-months old, in order to detect chemical modifications during the course of the disease. Furthermore, six one-month old GAA-KO $6^{neo}/6^{neo}$ mice were injected with AAVrh10-CAG-rhGAA (three mice -/- AAV10) or AAV9-CAG-rhGAA (three mice -/- AAV9). At twelve months, injected mice were euthanised. Finally, a total of 18 mice were included in the study, 6 mice euthanised at one-month old and 12 mice euthanised at twelve-months old. After anaesthesia and analgesia, mice were perfused intracardially in the left ventricle with 1 mL of phosphate buffer saline followed by 9 mL of 4 % paraformaldehyde (PFA) in order to carry out exsanguination and a first fixation of the tissues of interest. The heart was then removed and fixed for 48 h in a 4 % PFA bath at 4 °C.

Once the hearts were fixed, they underwent several dehydration baths (from alcohol to cyclomethylhexane) and were included in paraffin. Hearts were cut with a microtome (Microm model HM355S, MM France), which cut the paraffin blocks with a very high precision. The sections of 10 µm depth were placed on zinc selenide windows (ZnSe, 13 mm in diameter, Crystran, UK) for IR microspectroscopy and on quartz slides for DUV imaging.

Tissue processing for histology

Paraffin-embedded 10 µm serial sections were stained with PAS and observed using the Nikon Eclipse 90i® microscope (Nikon, Champigny, France) and NIS-element software.

Immunohistochemistry

Paraffin-embedded sections were used to investigate the cellular localisation of GAA in the cardiac muscle. Immunohistofluorescence was performed with a rabbit anti-GAA antibody (home-made) on dewaxed sections. Briefly, primary antibody was incubated overnight at 4 °C after permeabilisation and the secondary antibody labelled with Alexa® red 555 (Life Technologies; 555A21429-1/500) was incubated for 1 h at room temperature. Observations and image acquisition were performed with a confocal laser scanning microscopy (LSM 780 Zeiss, Marly le Roi, France).

Synchrotron source and methods of acquisition

FT-IR microspectroscopy

Dewaxed cardiac muscle cross-sections were studied from one-month old animals (three Wt and three

Pompe mice) and from twelve-month old animals (three mock-treated Pompe mice, three AAV9-treated Pompe mice, three AAV10-treated Pompe mice and three Wt mice). Conventional FT-IR microspectroscopic imaging was performed at the SMIS beamline (Spectroscopy and Microscopy in the IR using Synchrotron SOLEIL, Gif/Yvette, France) using an IR microscope (Nicolet iN10, Thermo Scientific, USA) to collect chemical information at medium resolution in order to perform an IR mapping of the whole cardiac cross-section. Spectra were acquired in transmission mode with an aperture of $25 \times 25\ \mu m^2$ and steps of 25 µm. Glycogen content was determined by the area under the curve for the glycogen peaks and ratioed against the amide I peak area using Omnic software (Thermo Scientific). High spatial resolution IR spectral maps were then collected using the SMIS beamline. All spectra were recorded in transmission mode using a $10 \times 10\ \mu m^2$ dual-path single-aperture on a Continuum XL microscope (Thermo Scientific). The microscope comprises a motorised sample stage and a liquid-nitrogen-cooled mercury cadmium telluride (MCT-A) detector (50 µm element size). The microscope operates in confocal mode using a 32× infinity-corrected Schwarzschild objective (*NA* = 0.65) and a matching 32× condenser. Two approaches to the investigation were performed: i) point mapping including fibres and connective tissue exploration and ii) single point exploration allowing single fibre analysis without connective tissue. Individual spectra were saved in log (1/*R*) format at $8\ cm^{-1}$ spectral resolution, with 128 co-added scans encompassing the mid-IR region from $4000\ cm^{-1}$ to $650\ cm^{-1}$. All IR spectra were pre-processed and submitted to multivariate data analysis (The Unscrambler X 10.3, CAMO Process AS, www.camo.com). Spectral data were first baseline corrected and unit vector normalised. Second derivatives of the spectral data were assessed (nine-point Savitzky–Golay filter) to enhance the spectral resolution of the absorption bands. The second derivative IR spectra pre-multiplied by −1 were analysed by applying principal component analysis (PCA). The computation of principal components was based on the non-linear iterative projections by alternating least-squares algorithm. While the score plots allowed a comparison of the IR spectra, the corresponding loading plots revealed the main characteristic absorption bands behind the clustering of the spectra.

Synchrotron DUV fluorescence imaging

Dewaxed cardiac muscle cross-sections (10 µm) from twelve-month old animals were studied (three AAV9-treated Pompe mice and three mock-treated Pompe mice-/- PBS). The sections were placed on circular quartz slides for DUV imaging (diameter 12.7 mm, ESCO optics, New Jersey, USA). The DISCO beamline at SOLEIL synchrotron has an experimental imaging station on which the bending magnet delivers DUV radiation in the visible, continuously tuneable from 180 nm to 600 nm (1.2–20 eV). Many aromatic groups and many enzymes naturally luminesce under UV excitation without external markers. This makes the DISCO beamline an instrumentation adapted to the *in situ* study of samples derived from cell biology and biomedine, with a desire to exploit the intrinsic fluorescence of molecules.[35,41,42] The DISCO beamline imaging station consists of two microscopes. The first microscope, so-called Telemos, is a full-field fluorescence microscope. A second microscope, so-called Polypheme, is a microspectroscopic microscope devoted to hyperspectral imaging. The full-field sDUV imaging system is constructed around a Zeiss Axio Observer Z1 (Zeiss) inverted microscope constructed with quartz-only optics. The white beam of DISCO beamline at Synchrotron SOLEIL is monochromatised by an iHR320 (Jobin-Yvon Horiba) before coupling with the entrance of the modified Zeiss Axio Observer Z1, the monochromatic beam was settled at 280 nm. A sharp dichroic mirror transmitting only above 300 nm (Omega Optical) reflected the incident light before focussing onto the sample through a Zeiss Ultrafluor 40 (*NA* = 0.6, glycerine immersion). Emission was recorded with a Pixis 1024-BUV camera (Princeton Instruments) after passing through a series of bandpass filters [307–323 nm, 327–353 nm, 370–410 nm, 412–438 nm and 420–480 nm (Semrock)]. These channels were chosen according to the aromatic groups which fluoresce at these wavelengths and which can be associated in their interpretation with the presence of different amino acids or proteins. Thus, we assigned the first channel to the presence of tyrosine, the second and third to the presence of tryptophan and finally the last two to the presence of collagen cross-links in the tissue (Figure 6). Fluorescence images where typically recorded in a few seconds exposure. Power measured on the sample was close to $\mu W\ cm^{-1}$. The whole system is controlled via Micro-Manager.[43,44] The acquisitions were made with a ×10 lens allowing mosaics to be made and reconstructing a large image representa-

tive of a cross-section of the heart's size of the field. Five large images were acquired per sample. The images were analysed using Fiji software.[45] These images needed to be contrasted and coloured artificially by the software to be comparable and interpretable in a clearer and more precise way. The same contrast has been applied to all images. The intensity of fluorescence on the images increases from green to violet to orange (blue orange lookup table in Fiji). Ratios between images acquired in two different channels allow the expression of one element to be followed in relation to another and thus show biological interest. Images were divided following several combinations and four of them revealed significative difference between treated and untreated cardiac samples. Results are expressed as means ± standard deviation (sd). Effects of heart region analysed (septum, right and left ventricles) and experimental conditions (307–438 nm) on the percentage of fluorescent area have been evaluated with linear mixed-effects models. The theory of parametric estimation provides principles to compare different experimental situations. A significant difference was considered to exist when $p < 0.05$. Statistical analysis was performed using non-linear mixted effect packages in R software (R Core Team).

In UV fluorescence microspectroscopy, the excitation wavelength was at 280 nm and the recovery of the fluorescence was carried out between 300 nm and 550 nm. One hundred spectra were collected per region, i.e. between 200 and 300 spectra per animal with three animals per condition (AAV9 treated and mock-treated Pompe mice). Spectra were pre-processed and submitted to multivariate data analysis (The Unscrambler).

Results

Investigation of Pompe disease status by FT-IR microspectroscopy

Images of whole cardiac muscle sections were first recorded at medium spatial resolution ($25 \times 25\ \mu m^2$) using an iN10 microscope equipped with a thermal IR source. FT-IR spectral maps measured on cardiac muscle sections from one-month old and twelve-month old Pompe mice were compared with those of Wt animals. Figure 1a shows the representative raw IR spectra obtained from the cardiac muscle fibre of Wt mice (green and blue lines) and Pompe mice (orange and red lines), respectively aged one month and twelve months. The absorption intensities of the peaks at 1025 cm^{-1}, 1080 cm^{-1} and 1152 cm^{-1}, that originate from the C–O stretching vibrations of glycogen,[46] are distinctly stronger in Pompe mice at the early stage of the disease (one-month old) and are greatly increased in adult Pompe mice (twelve-month old) compared to the Wt animals.

Since the cardiac muscle sections comprised large empty areas devoid of any tissue, different tissue-filled areas were recorded sequentially and the image was then reconstituted by matching the spectral information of each single area to reconstruct a larger image. The ratio between the area under the glycogen peaks and the area under the amide I peak was used to normalise the samples' thickness heterogeneity in the chemical maps. Red hues indicated regions with high glycogen content; green hues indicated medium glycogen content while blue hues indicated low glycogen content (Figure 1b; ii, iv). Infrared microspectroscopy imaging enabled a sensitive detection of glycogen accumulation in comparison with PAS staining which did not allow a clear discrimination between Wt and Pompe cardiac muscle at one month (Figure 1b; i, iii). IR microspectroscopy imaging showed that no specific glycogen tissue compartmentalisation was present in the heart of one-month old Pompe mice (Figure 1b).

Synchrotron FT-IR microspectroscopy

The SOLEIL synchrotron radiation source was then used to achieve a spatial resolution compatible with the measurement of individual muscle fibres ($10 \times 10\ \mu m^2$) and to maintain a high signal-to-noise ratio necessary for multivariate analysis. Analyses were carried out in the heart pillar area in order to get information about glycogen storage in numerous transverse fibres at the single cell level. Indeed, cardiac muscle cells are very close and dense in the pillar area with a minimum size close to 10 µm and a thin connective tissue between the fibres requiring high spatial resolution synchrotron investigation to analyse cells individually.

The spectra were analysed by PCA and the results were represented by the score plot in which one point corresponds to one fibre spectrum and by the loading plot where the contribution of each wavenumber in the clustering of the spectra is explained (Figure 1c, d). Band assignments in the IR spectra was tentatively done according to the literature.[47–49] Three clusters can be separated along the PC-1 axis in the score plot (Figure 1c) and the loading plot showed the strong weight of the bands for glycogen

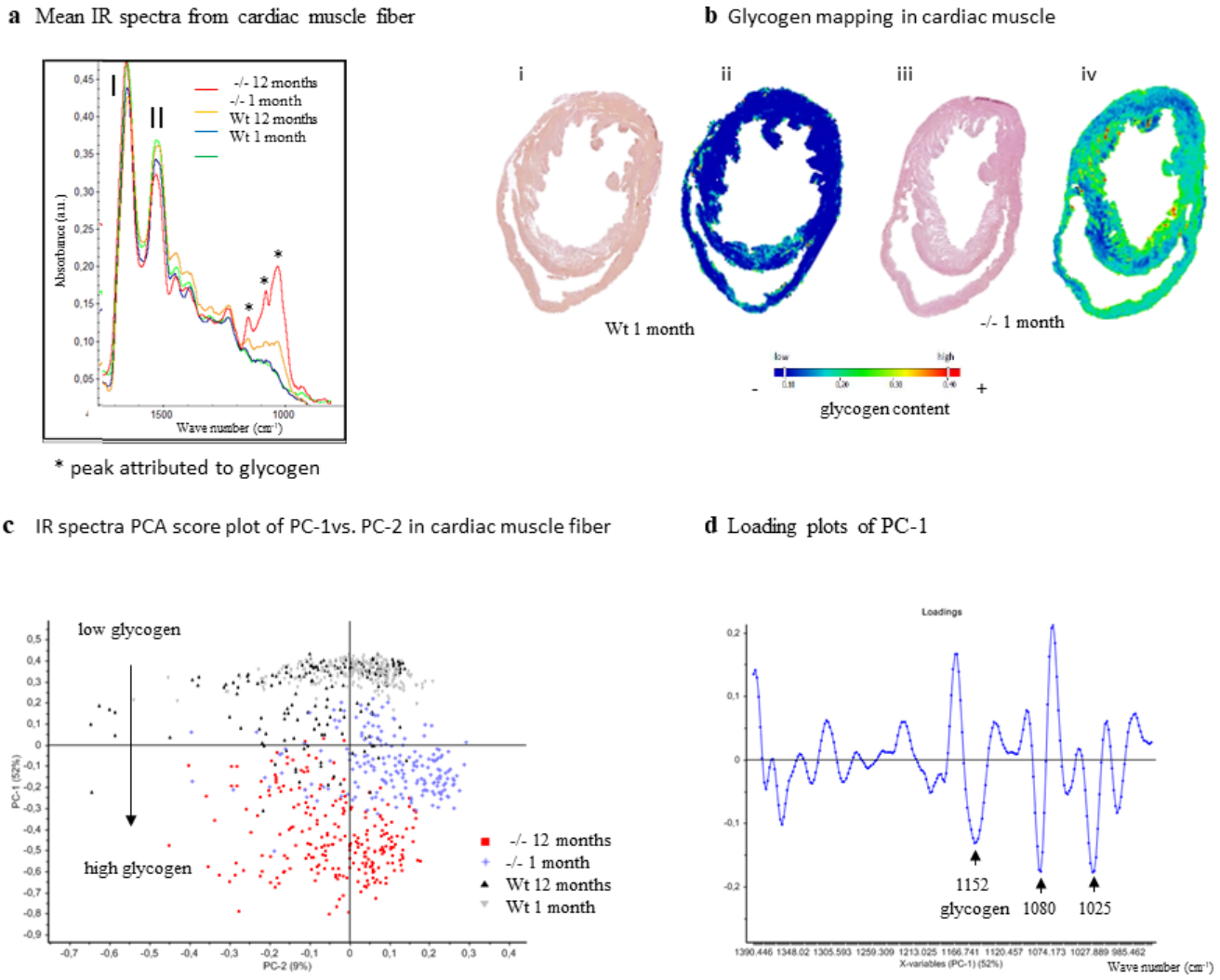

Figure 1. (a) Example of mean IR spectra obtained from cardiac muscle fibre of Wild type (Wt) and Pompe mice (-/-). Spectra from 1-month and 12-month old Wt are represented, respectively, by the green and blue curves. Spectra from 1-month Pompe mice (-/- 1 month) and 12-month old Pompe mice (-/- 12 months) are represented, respectively, by the orange and red curves, (*) three peaks (1152, 1080, 1025 cm^{-1}) attributed to glycogen. Spectra integration was performed on Omnic software, the area of glycogen peak was reported to the area of amide I peak. (b) (i) Periodic acid Schiff (PAS) staining of cardiac muscle sections from Wt and (iii) from Pompe mice. (ii) Glycogen mapping by IR microspectroscopic imaging in cardiac muscle from Wt and (iv) from Pompe mice performed from spectra integration described in (a). (c) PCA score plot realised from the second derivative (multiplied by −1) of IR spectra between 1400 cm^{-1} and 950 cm^{-1}. 1-month and 12-month old Wt animals were merged in the same cluster on the positive side of PC-1 axis, spectra from 1-month old Pompe animals are located mostly on the negative side of the plot axis, 12-month old Pompe animal spectra were all located on the negative side of the plot axis with higher negative values. (d) Loading plot showed spectral regions associated with chemical functional groups responsible for the clustering seen in the scores plot (glycogen: 1152, 1080, 1025 cm^{-1}), the higher glycogen signal was associated with the spectra of the Pompe animals.

at 1025 cm^{-1}, 1080 cm^{-1} and 1152 cm^{-1} in the clustering (Figure 1d). One-month and twelve-month old Wt mice were grouped in the first cluster (grey and black markers). One-month old Pompe mice (light blue markers) with a moderated elevation of the bands assigned to the carbohydrates of glycogen (1152 cm^{-1}, 1080 cm^{-1}, 1025 cm^{-1}) constituted a second cluster and finally twelve-month old Pompe mice (red markers) were grouped in a third cluster with stronger glycogen bands. There was no or little overlap between the Pompe and the Wt clusters, showing that most Pompe muscle fibres were affected by the increase in glycogen storage from as early as one

month, and that almost no Wt fibres had significantly higher glycogen levels. The spectra of cardiac fibres from the twelve-month old and one-month old Pompe mice showed very little overlap, evidencing a large increase in the glycogen level and suggesting that different stages in the progression of the disease may exist. In the loading plot, a small peak at around 1350 cm^{-1} appeared correlated with the stronger C–O peaks from glycogen. This might be tentatively assigned to the C–H deformation from CH_3 generally found at 1380 cm^{-1} and this could indicate a change in the lipid concentration associated with the change in glycogen storage. Alternatively, this could be assigned to the C–H deformation from CH_2 of beta-anomers at 1370 cm^{-1} that can be detected in pure glycogen spectra.

Multivariate data analyses were also performed on the 3600–1200 cm^{-1} wavenumber range to exclude the main bands of glycogen capable of masking new discriminant markers of the pathology and of the therapy response. The data analyses were focused on three parts of the spectra: the 3600–2800 cm^{-1} range for CH investigation associated with lipids but also NH (3300 cm^{-1}) and OH (3400–3600 cm^{-1}), the 1780–1200 cm^{-1} range for exploration of amide I, II, III and lipid esters, and the 1480–1180 cm^{-1} range for amide III and collagen (1320–1360 cm^{-1}) investigations. PCA results were represented by the corresponding score and loading plots (Figure 2). For the 3600–2800 cm^{-1} range (Figure 2a), separation of twelve-month old mice from one-month old mice was obtained along the PC-1 axis with the main differences at 2908, 2860 and 2840 cm^{-1} observed on the loading plot. The peaks at 2919 and 2850 cm^{-1} were not interpreted since the tissues were first paraffin embedded and then dewaxed. Only CH_3 peaks were considered informative. Furthermore, PCA performed on the 1780–1200 cm^{-1} range highlighted a separation along the PC-1 axis between twelve-month old Pompe mice (80 % below the PC-1 axis) and one-month old mice (for both one-month old Wt mice and one-month old Pompe mice, 86 % above the PC-1 axis). Twelve-month old Wt mice were distributed on either side of the PC-3 axis (59 %/41 %) and on either side of the PC-1 axis (54 %/46 %) (Figure 2b). Twelve-month old Pompe mice formed a cluster along the PC-3 axis (88 % of twelve-month old Pompe mice separated along the PC-3 axis). A shift of the amide I toward low frequencies (shown by the peak at 1630 cm^{-1} in PC-1 loadings) was related to the separation of the twelve-month old Pompe mice by PCA. This suggested that changes in the proteins, either conformational, intermolecular aggregation or *de novo* expression, were implicated in the separation of the cluster. We focused on the analysis of collagen which exhibits a strong signal at 1637 cm^{-1} arising from the triple-helix.[50]

Assessment of AAV gene therapy efficiency by FT-IR microscopy

The objective of our IR experiments was also to demonstrate the potential of this new approach to assess AAV gene therapy on Pompe cardiac muscle.

We first mapped the distribution of glycogen in the whole cardiac muscle of mock-treated Pompe mice (-/- PBS), AAV9-treated Pompe mice (-/- AAV9), AAV10-treated Pompe mice (-/- AAV10) and Wt mice using the iN10 imager (Figure 3). Thanks to glycogen spectroscopic mapping, we demonstrated that glycogen storage was strongly decreased in cardiac muscle of AAV9-treated Pompe mice compared to AAV10-treated Pompe mice (Figure 3b). Furthermore, thanks to the sensitive FT-IR glycogen mapping and GAA immunohistochemistry, our study allowed us to demonstrate a partial concordance between the GAA-rich area and the poor glycogen area on AAV9-treated Pompe cardiac section (Figure 3c). GAA expression was particularly high in the papillary muscles from AAV9-treated Pompe. This GAA-rich area was associated with a low glycogen concentration (Figure 3c).

Higher-resolution IR microspectroscopy analyses were carried out in the heart papillary muscles using synchrotron radiation. The papillary muscles area was chosen for its homogeneous structure (transversal fibres exclusively). PCA performed on the 1400–950 cm^{-1} range revealed a clear separation along the PC-1 axis between the AAV9-treated and the AAV10-treated mice in the spectral area specific to glycogen (1025, 1080 and 1152 cm^{-1}; Figure 4). Furthermore, PCA performed on the 1450–1300 cm^{-1} range revealed that 88 % of twelve-month old mice (both Pompe and Wt) were located above the PC-2 axis whereas 63 % of AAV10-treated mice and 40 % of AAV9-treated mice were situated below PC-2 associated with 1403 cm^{-1}, 1375 cm^{-1} and 1332 cm^{-1} (Figure 5).

Assessment of AAV gene therapy efficiency by DUV microscopy/microspectroscopy

The DISCO imaging beamline devoted to synchrotron radiation UV fluorescent microscopy was used to explore the autofluorescence of cardiac tissue.[35,41] We elected to investigate tyrosine, tryptophan and collagen cross-

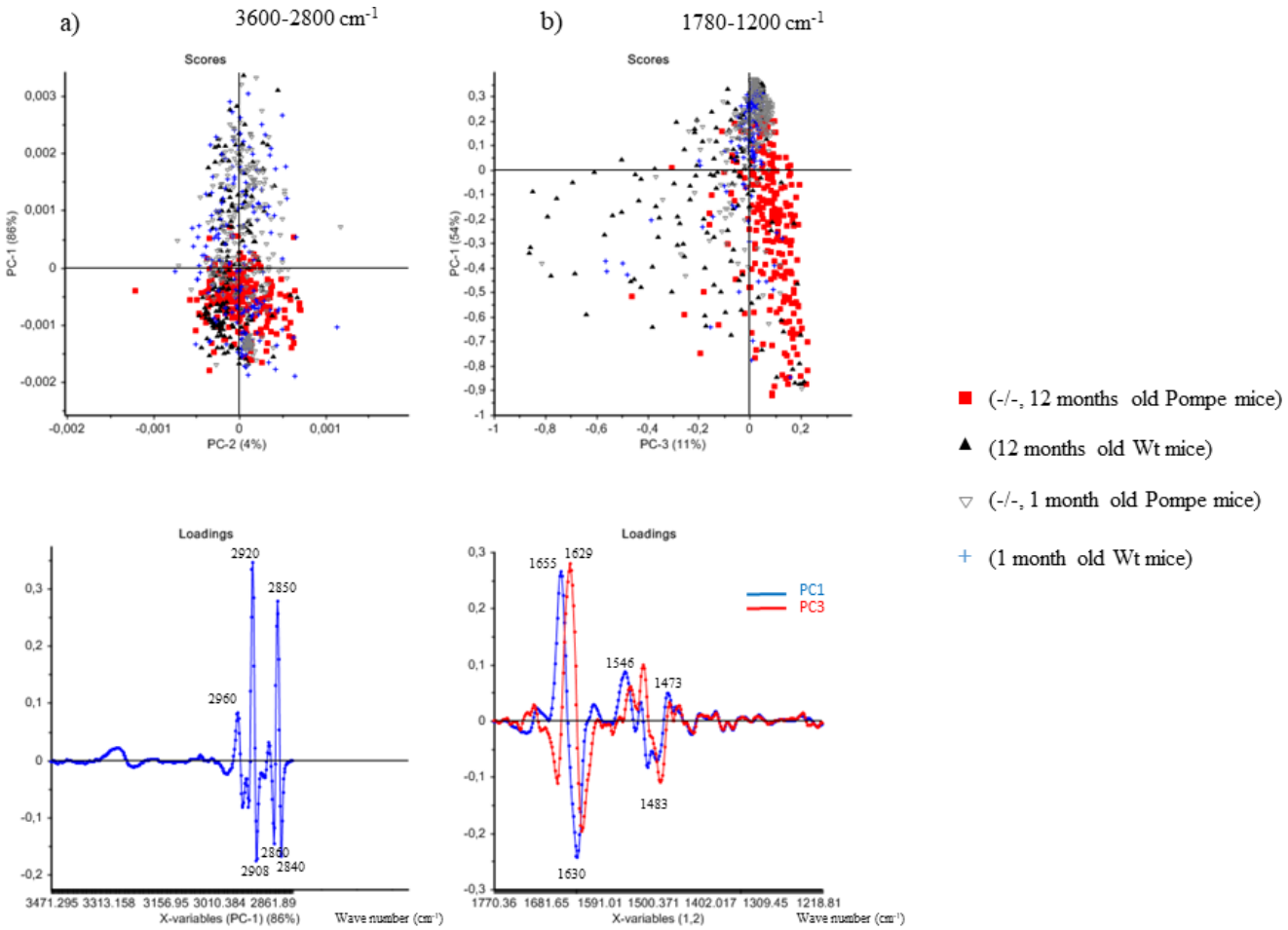

Figure 2. (a) PCA score plot realised from the second derivative (multiplied by −1) of IR spectra between 3600 cm^{-1} and 2800 cm^{-1}. 12-month old Pompe animals were all located on the negative side of PC-1 axis with the main differences at 2908, 2860 and 2840 cm^{-1} observed on the loading plot. (b) PCA score plot realised from the second derivative (multiplied by −1) of IR spectra between 1780 cm^{-1} and 1200 cm^{-1}. Two clusters were separated in the score plots, i) along the PC-1 axis, separation of 1-month old mice from 12-month old Pompe mice with strong differences in the clustering on 1655 cm^{-1} (high weight for 1-month old mice) and 1630 cm^{-1} (high weight for 12-month old Pompe mice), ii) along PC-3 axis, 12-month old Pompe mice formed a cluster at right of PC-3. 12-month old Wt mice were distributed from either side of PC-3 and PC-1 axis.

links (pentosidine) autofluorescence using sDUV microspectroscopy with 280 nm excitation. Figure 6 shows a series of images obtained from cardiac muscle sections showing the different patterns of fluorescence mapping obtained using five complementary filters (described in Figure 6a). The ratio between the image obtained with filter 2 (327–353 nm) and the image obtained with filter 1 (307–323 nm) gave a resultant image attributed to tryptophan/tyrosine ratio (image not shown), and the ratio between the image obtained in filter 2 (327–353 nm) and the image obtained in filter 4 (412–438 nm) gave a resultant image attributed to tryptophan/collagen cross-links ratio (Figure 7). These operations allowed the results to be rationalised and to bypass a possible surface roughness effect (Figure 7a–c). Fluorescence of rationalised images was analysed separately in the right ventricle, left ventricle and in the septum by the selection of regions of interest (ROI) and by using a determined threshold for image analysis. Histograms shown in Figure 7d–e showed significant differences between mock-treated Pompe mice and AAV9-treated Pompe mice in the right ventricle for the images resulting from tryptophan/collagen cross-links ratio and tryptophan/tyrosine ratio with a level of risk tolerance equal to 5% and a p-value less than 0.05.

Hyperspectral imaging using highly sensitive and high-resolution UV microspectroscopy analyses was carried

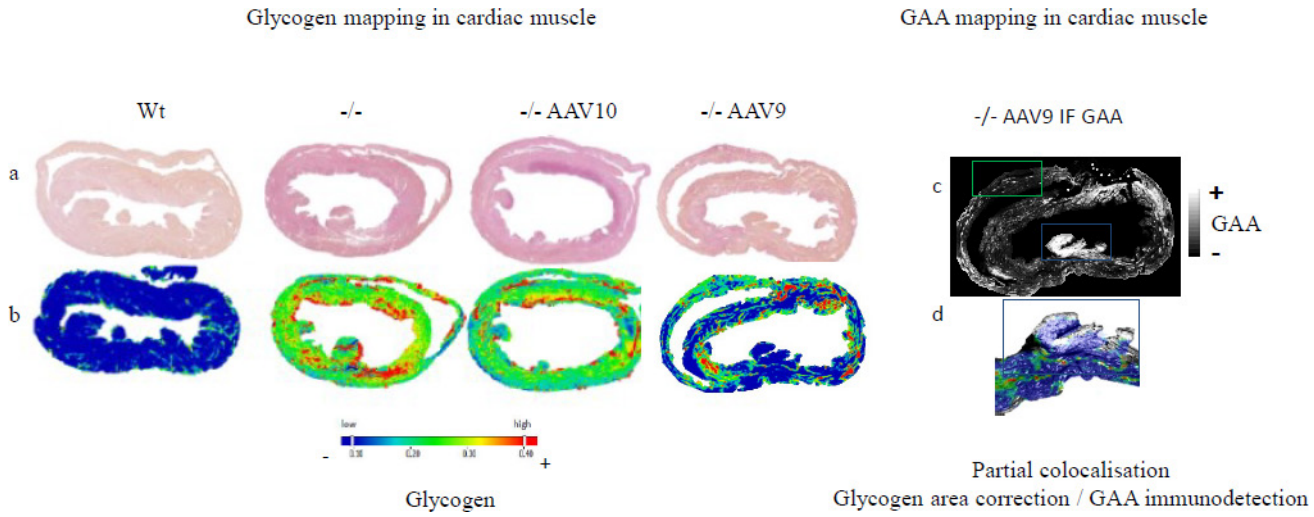

Figure 3. Representative sections of cardiac muscle from 12-month old mice. (a) PAS staining of cardiac muscle of Wild type mouse (Wt), mock-treated Pompe mouse (-/-), AAV9-treated Pompe mouse (-/- AAV9), AAV10-treated Pompe mouse (-/- AAV10). The glycogen storage appears in purple on a light pink background. (b) Infrared chemical mapping of glycogen in cardiac muscle of Wt, mock-treated Pompe mouse (-/-), AAV9-treated Pompe mouse (-/- AAV9), AAV10-treated Pompe mouse (-/- AAV10). The relative concentration of glycogen was determined from the area under the curve for the glycogen pic centred at 1080 cm^{-1} and normalised versus the protein pic area centred at 1654 cm^{-1}. (c) Acid alpha-glucosidase immunolabeling on AAV9-treated Pompe mice cardiac muscle section (-/- AAV9). (d) partial colocalisation between area with glycogen correction and GAA immunodetection.

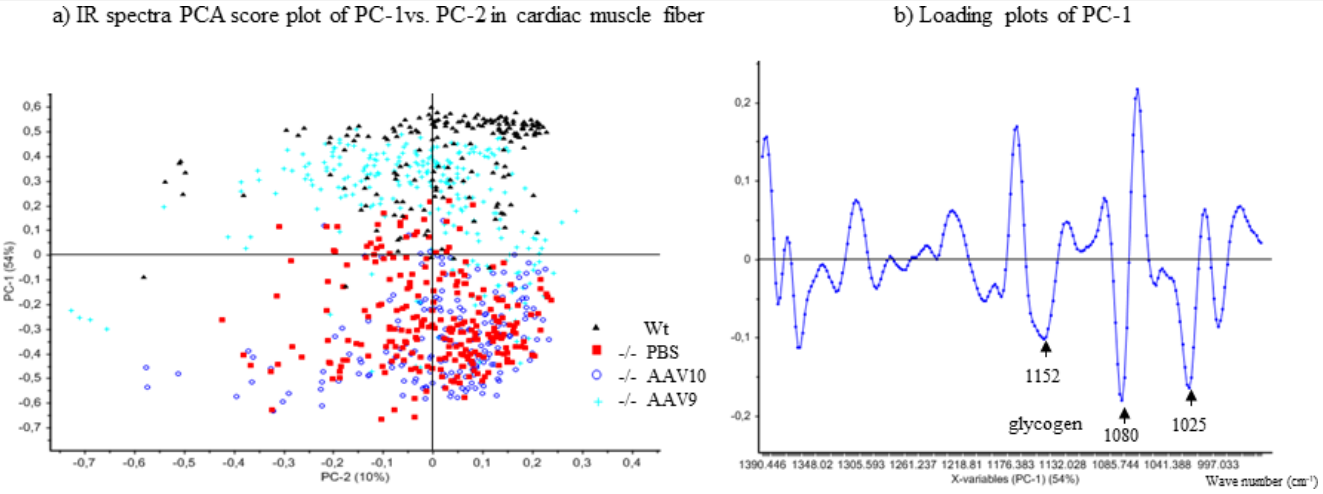

Figure 4. PCA scores plot realised from IR spectral data obtained between 1400 cm^{-1} and 950 cm^{-1} for 12-month old mice: Wild type (Wt), Pompe mice (-/- PBS), AAV9-treated Pompe mice (-/- AAV9) and AAV10-treated Pompe mice (-/- AAV10). Wt and AAV9-treated Pompe mice (-/- AAV9) were merged in the same cluster on the positive side of axis with low content of glycogen whereas mock-treated Pompe mice (-/-) and AAV10-treated Pompe are merged and located mainly on the negative side of the plot axis with high glycogen content. (b) Loading plots showed spectral regions associated with chemical functional groups responsible for the clustering seen in the scores plot (glycogen: 1152, 1080, 1025 cm^{-1}).

out in mock-treated and in AAV9-treated Pompe mice. Three distinct areas were investigated in cardiac muscle from three mock-treated Pompe mice (-/- PBS) and three AAV9-treated Pompe mice (-/- AAV9). The GAA-rich area from AAV9-treated Pompe mice was selected from serial tissue sections previously immunolabeled with anti-GAA antibody. Immunolabeling of GAA showed a heterogeneous expression in the tissue (Figure 8a). PCA

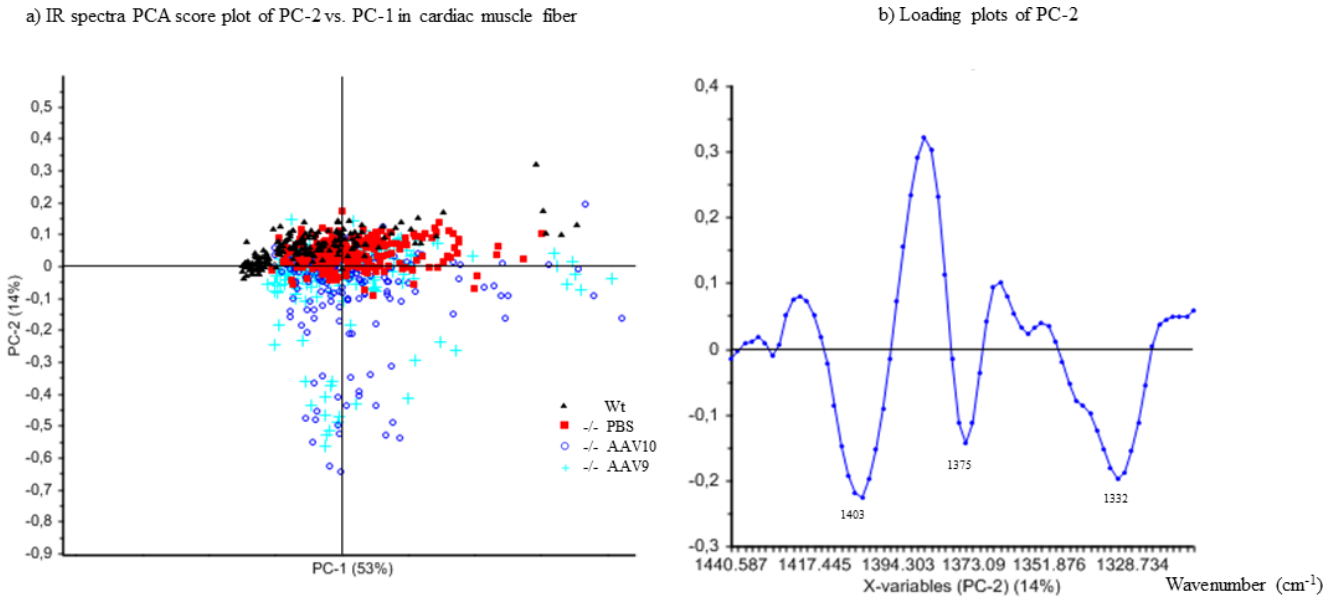

Figure 5. (a) PCA scores plot realised from IR spectral data obtained between 1450 cm^{-1} and 1300 cm^{-1} for 12-month old mice: Wild type (Wt), Pompe mice (-/- PBS), AAV9-treated Pompe mice (-/- AAV9) and AAV10-treated Pompe mice (-/- AAV10). Wt and mock-treated Pompe mice (-/-) were merged in the same cluster on the positive side, whereas mainly AAV9-treated Pompe mice and AAV10-treated Pompe were located on the negative side of the plot axis. (b) Loading plots showed spectral regions associated with chemical functional groups responsible for the clustering seen in the scores plot (1403, 1375, 1332 cm^{-1}).

was performed on the DUV spectra and the results were represented as score plots (Figure 8b). The discrimination of clusters was possible using the score plot, and the loading plot revealed that clustering was based on the characteristic band of tryptophan (Figure 8c). In the score plot, each red spot corresponded to an emission spectrum obtained from mock-treated Pompe mice fibres, whereas each blue/purple spot (purple, blue, light blue) corresponded to an emission spectrum from AAV9-treated Pompe mice fibres from three animals. One hundred spectra were analysed for each condition. Red spots formed an elongated cloud along the PC-1 axis, showing a strong variability in the 310/348 nm ratio, whereas blue/purple spots formed three distinct clouds of points along the PC-3 axis with two clouds located in the positive part of the plot (high content in tryptophan). The two positive clouds represented spectra obtained from one AAV9-treated Pompe mice (purple points; Figure 8b) and could be due to the presence of GAA. The heterogeneity of the clusters for the AAV9-treated Pompe mice, obtained with PCA, could be related to the heterogeneity of hGAA content detected in the serial tissue sections by hGAA immunolabeling. The hGAA detection from its tryptophan autofluorescence UV spectra would be in accordance with the high content of tryptophan residues in hGAA (21/952 amino acids).

Discussion

The efficacy of a rhGAA-AAV9 gene therapy on cardiac muscle of GAA-KO $6^{neo}/6^{neo}$ mice was demonstrated by using sDUV microscopy and sFT-IR microspectroscopies. From glycogen spectroscopic mapping, we demonstrated that glycogen storage was strongly decreased in cardiac muscle of AAV9-treated Pompe mice compared to AAV10-treated Pompe mice. These results are consistent with those obtained using biochemical glycogen assay performed on AAV9- and AAV10-treated Pompe cardiac muscles.[26] Furthermore, the heterogeneity observed inside the AAV9-treated Pompe mice cluster was in agreement with the variability of the glycogen storage correction previously described in AAV9-treated mice cardiac muscle from GAA and glycogen assay.[26]

The results are in accordance with previous studies published by Hordeaux *et al.*[26] that demonstrated a better efficiency of the AAV9 vector for the correction of cardiac muscle in Pompe disease by using conventional

a)

Emission Filter	Wavelength (nm)	Auto fluorescence
Filter 1	307-323	Tyrosine
Filter 2	327-355	Tryptophan
Filter 3	370-410	Tryptophan
Filter 4	412-438	Collagen
Filter 5	420-480	Collagen

b)

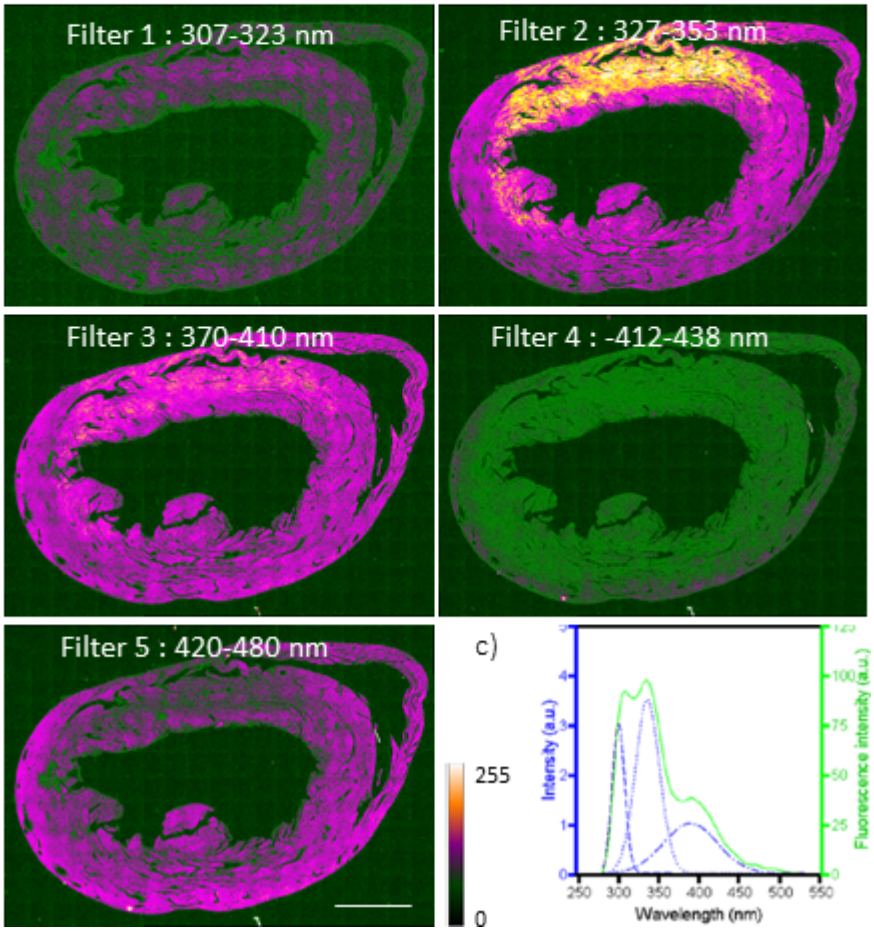

Figure 6. (a) Table with the list of emission filters used for the image acquisition and the corresponding autofluorescent components. (b) images of cardiac muscle section resulting from the acquisition with the different filters. (c) Fluorescence spectra of tyrosine, tryptophan, collagen. Scale bar, 400 µm.

approaches as glycogen biochemical assay, GAA enzymatic activity measurements and histological investigations.

The potential of synchrotron IR microspectroscopy is particularly well documented in the mapping of chemical modifications in pathological tissue,[32,51–54] but until now, no sFT-IR or sDUV spectroscopy has been performed to investigate the chemical changes in Pompe cardiac muscle.

By using high spatial resolution synchrotron methods and multivariate data analysis applied to IR spectral data, we have shown for the first time that it was possible to

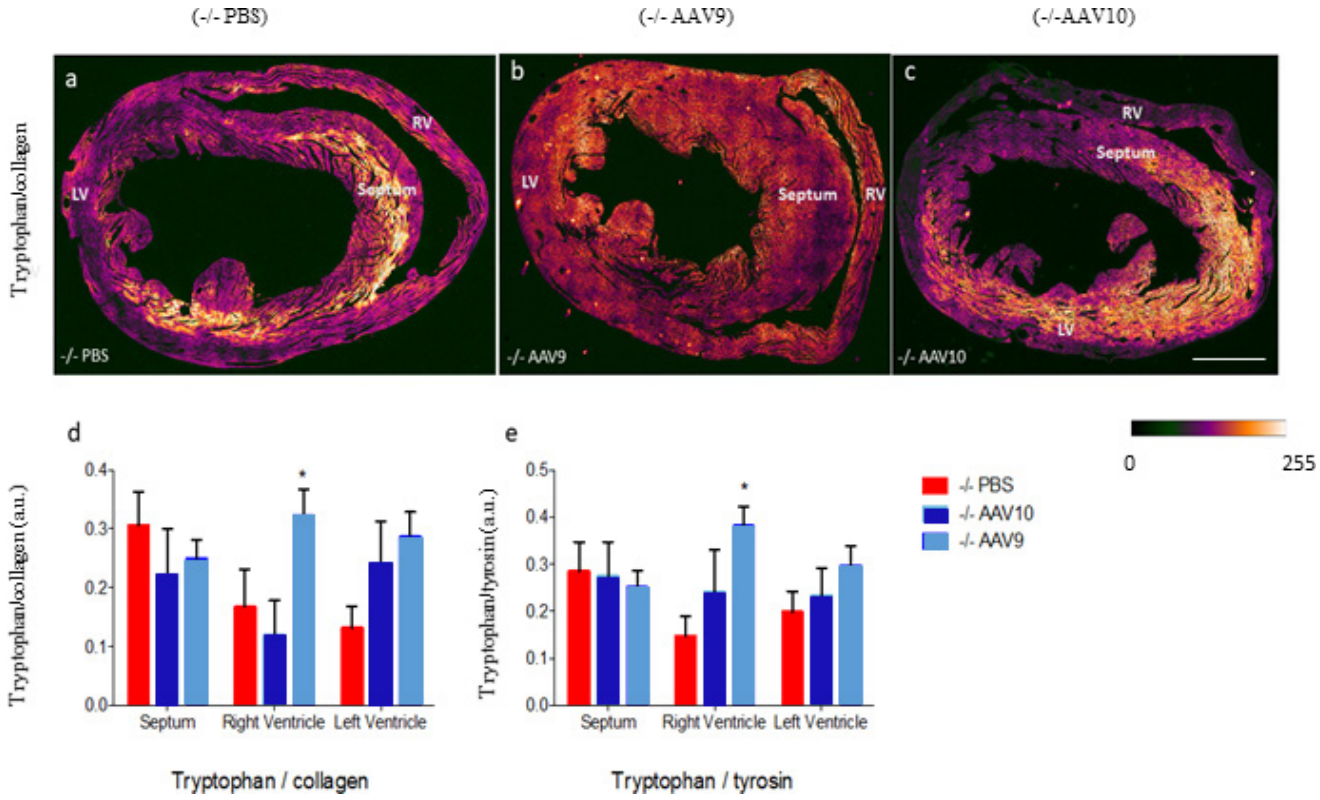

Figure 7. Representative cardiac muscle section from (a) mock-treated Pompe mice (-/-) tryptophan/collagen ratio. (b) AAV9-treated Pompe mice tryptophan/collagen ratio (-/- AAV9). (c) AAV10-treated Pompe mice (-/- AAV10) tryptophan/collagen ratio. Scale bar, 400 µm. (d–e) Fluorescence of rationalised images was analysed separately in right ventricle, left ventricle and the septum by the selection of regions of interest (ROI) and by using a common threshold for image analyses. Histograms of (d–e) showed significative differences between mock-treated mice and AAV9-treated mice in the right ventricle for the images resulting from (d) the tryptophan/collagen ratio and (e) the tryptopan/tyrosine with a level of risk tolerance equal to 5 % and a p-value less than 0.05. Statistical analyses were performed using linear mixed effects models with R software.

follow glycogen accumulation in the cardiac muscle from Pompe mice, fibre by fibre, thanks to the glycogen spectral signature. The power of the method was particularly demonstrated by the capability to separate clearly AAV9-treated Pompe mice and Wt mice from AAV10-treated Pompe mice and mock-treated Pompe mice by considering their differences in glycogen spectral intensities. Glycogen and GAA content are the two main biomarkers of Pompe disease currently analysed to follow the course of the disease and to assess the efficacy of therapies. These biomarkers are routinely analysed by performing biochemical assays and histopathological investigations consisting of glycogen PAS staining and GAA immunohistochemistry on tissue sections.[15,26,55–57] Glycogen PAS staining is based on the principle of periodic acid-induced oxidative cleavage of carbon-to-carbon bounds in 1,2-glycols to form dialdehydes reacting with fuchsin-sulphurous acid, which in turn combines with the basic pararosaline, yielding a magenta-like stain.[58] PAS staining could be used to quantify glycogen in tissue sections but the thickness of the sections has to remain constant to ensure the validity of the comparison of glycogen content between sections.[59] Different tissue types, thicknesses, hydration state or densities could affect the penetration rate of the stain and the accuracy of the quantification. On the other hand, infrared microspectroscopy offers the opportunity to study the glycogen mapping on tissue sections by investigating the intrinsic glycogen molecular vibration without adding any marker and with µm spatial resolution.[60–62] Thanks to the normalisation of glycogen bands with the amide I band, it is possible to account for the varying thickness of the sample, which was not possible from glycogen PAS staining. In this work, we only carried out a semi-quantitative assessment of glycogen concentration by measuring the glycogen/protein peak area ratio, but it would be possible to determine the exact

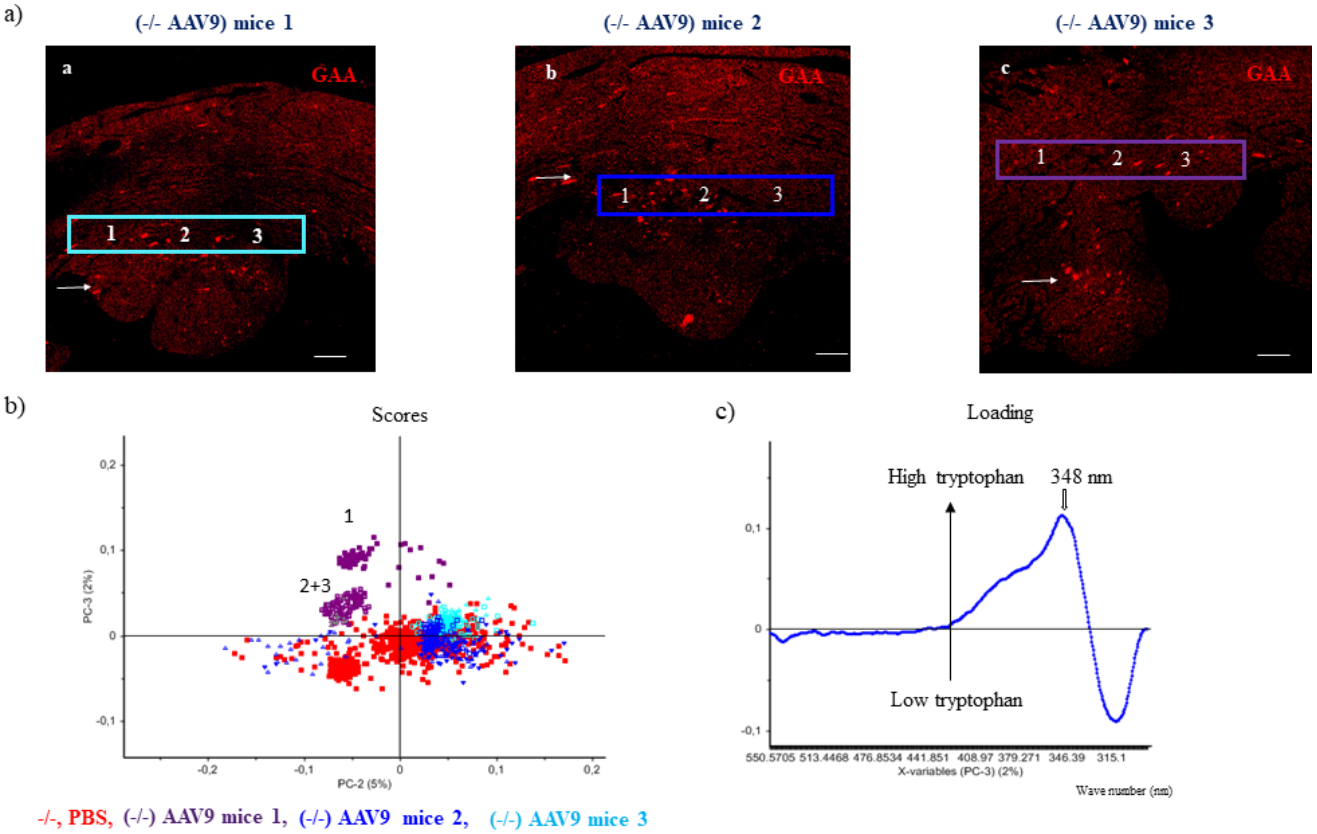

Figure 8. (a) Immunohistochemistry of GAA on cardiac muscle section for three AAV9-treated Pompe mice. GAA was detected in red fluorescence. Areas 1, 2, 3 corresponded to the area explored with UV microspectroscopy. Scale bar 200 µm. (b) PCA scores plot realised from UV spectral data obtained between 300 nm and 550 nm for cardiac muscle from three mock-treated and three AAV9-treated Pompe mice. Three distinct areas were investigated in each cardiac muscle. PCA methods allowed the discrimination of clusters based on the characteristic band of tryptophan. Each red spot corresponded to an emission spectrum obtained from total mock-treated mice fibres whereas each of the purple and blue clusters (purple, blue, light blue) corresponded to the emission spectrum from, respectively, the three AAV9-treated mice analysed. Red spots formed an homogenous cloud of points along the horizontal axis whereas blue/purple spots formed three distinct clouds of points with two clouds located in the positive part of the plot (high content in tryptophan represented in purple, a first cluster with data from area 1, a second cluster with data from area 2 + 3). The heterogeneity of the spectra obtained from the AAV9-treated Pompe mice could be related to the heterogeneity of hGAA detected in the serial tissue sections by hGAA immunolabeling. Spectra were pre-processed and submitted to multivariate data analysis (The Unscrambler, CAMO Process AS, www.camo.com). (c) Loading plot.

glycogen concentration in each of the cells from the same IR spectra by using multivariate regression methods (partial least squares regression, principal component regression, multivariate curve resolution alternating least squares etc.). It would be necessary to build a regression model with IR spectra from mixtures of proteins (e.g. cardiac muscle actin) and glycogen with a known concentration. Compared to the conventional methods, infrared microspectroscopy is a promising non-destructive method using a small quantity of tissue compatible with human tissue exploration.

The power of sFT-IR resides also in the fact that investigation of chemical changes is not restricted to the major biomarkers of a disease but could highlight a large panel of new minor and discriminant biomarkers. Thus, our experiments showed that the twelve-month old Pompe mice spectra could be separated from the other groups according to differences in the C–H bands intensity between 2960 cm^{-1} and 2840 cm^{-1}, assigned in the literature to asymmetric and symmetric C–H stretching vibrations of CH_3 (2956 cm^{-1} and 2874 cm^{-1}) and CH_2 (2900 cm^{-1} and 2852 cm^{-1}).[32] This discrimi-

nation of twelve-month old Pompe mice by their CH_3 peak intensity is compatible with the excessive accumulation of enlarged lysosomes in Pompe cardiac fibres well described in the literature.[63] Furthermore, our sFT-IR spectral analyses have shown that the bands associated with amide I, II and III were capable of discriminating the cluster of twelve-month old Pompe mice from the other groups. Twelve-month old Pompe mice spectra were characterised by a high positive signal at 1630 cm^{-1} attributed to the β-sheets structure of proteins in the literature.[64] This high content of β-sheet in cardiac fibres of Pompe mice could be a sign of protein denaturation and/or aggregation and is in accordance with the complete disorganisation of the Pompe myofibrils largely described in the literature.[26,63] On the other hand, we have shown that 60 % of AAV9-treated animals formed a cluster associated with the bands at 1403 cm^{-1}, 1375 cm^{-1} and 1332 cm^{-1} related to lipid C–H.

In addition, our results have demonstrated that sDUV microspectroscopy was able to discriminate the AAV9-treated Pompe mice from the other animals by both their high tryptophan/collagen ratio and tryptophan/tyrosine ratio, especially in the right ventricle. sDUV radiation has been described as a method with a high potential to detect autofluorescence of aromatic amino acid.[36] The higher content of tryptophan observed in the right ventricle could be compatible with the presence of hGAA (21 tryptophan for 952 amino acids). GAA immunodetection performed on cardiac muscle sections have shown the presence of GAA in the right ventricle but not exclusively in this area (Figure 3). On the other hand, hyperspectral imaging analyses revealed a clustering of spectra from one AAV9-treated mouse based on the characteristic band of tryptophan, which could be due to the presence of GAA detected by immunohistofluorescence in serial cardiac muscle section. The presence of tryptophan, highlighted by sDUV, needs to be investigated further to establish a direct relation with the presence of GAA in the tissue.

In conclusion, these dual complementary approaches using synchrotron IR and DUV radiations represent promising, label-free, non-destructive and unbiased methods to investigate the course of the disease as well as to assess the efficacy of new therapeutic strategies with high sensitivity and robustness in animal models and in human patients. Thanks to the high resolution of synchrotron light and because the spectral analyses were performed *a priori*, we have identified unexpected changes in sFT-IR spectra and a new autofluorescent profile in sDUV that can be used to characterise the course of Pompe disease and the efficiency of therapy. Furthermore, thanks to this non-invasive method, unlabelled samples can, after being analysed spectroscopically, be used for histopathological analysis or mass spectrometry imaging analysis for a deeper understanding of the pathophysiology.

Acknowledgements

We thank the vector core of the Atlantic Gene Therapies Institute (AGT) in Nantes for the preparation of the rAAV vectors, Véronique Blouin and Philippe Moullier (INSERM UMR1089) for vector production and fruitful discussions and the technical staff of Oniris rodent facility for animal care. The authors have used the SMIS beam line (proposal 20140468) and DISCO beam line (proposal 20150217) at the Synchrotron SOLEIL. They would like to recognise assistance from SMIS and DISCO beamline staff. This work was supported by grants from the Région Pays de la Loire and the National French Academy of Medicine and "Investissement d'Avenir-ANR-11-INBS-0011"–NeurATRIS: A Translational Research Infrastructure for Biotherapies in Neurosciences (MAC).

References

1. H.G. Hers, "Alpha-glucosidase deficiency in generalized glycogenstorage disease (Pompe's disease)", *Biochem. J.* **86,** 11–16 (1963). https://doi.org/10.1042/bj0860011
2. R. Hirschhorn and A.J.J. Reuser, "135: Pompe disease: glycogen storage disease type II, acid α-clucosidase (acid maltase) deficiency", in *The Online Metabolic and Molecular Bases of Inherited Disease*, Ed by A.L. Beaudet, B. Vogelstein, K.W. Kinzler, S.E. Antonarakis, A. Ballabio, K.M. Gibson and G. Mitchell. McGraw-Hill Medical. https://ommbid.mhmedical.com/content.aspx?sectionid=62641992&bookid=971
3. F. Martiniuk, A. Chen, A. Mack, E. Arvanitopoulos, Y. Chen, W.N. Rom, W.J. Codd, B. Hanna, P. Alcabes, N. Raben and P. Plotz, "Carrier frequency for glycogen storage disease type II in New York and estimates of affected individu-

als born with the disease" *Am. J. Med. Genet.* **79,** 69–72 (1998). https://doi.org/10.1002/(SICI)1096-8628(19980827)79:1<69::AID-AJMG16>3.0.CO;2-K

4. M. Ausems, J. Verbiest, M. Hermans, M.A. Kroos, F.A. Beemer, J.H.J. Wokke, L.A. Sandkuijl, A.J.J. Reuser and A.T. van der Ploeg, "Frequency of glycogen storage disease type II in The Netherlands: implications for diagnosis and genetic counselling", *Eur. J. Hum. Genet.* **7,** 713–716 (1999). https://doi.org/10.1038/sj.ejhg.5200367
5. A.T. van der Ploeg and A.J. Reuser, "Pompe's disease", *Lancet* **372(9646),** 1342–1353 (2008). https://doi.org/10.1016/S0140-6736(08)61555-X
6. J.J. Martin, T. de Barsy, F. van Hoof and G. Palladini, "Pompe's disease: an inborn lysosomal disorder with storage of glycogen. A study of brain and striated muscle", *Acta Neuropathol.* **23(3),** 229–244 (1973). https://doi.org/10.1007/BF00687878
7. H.M. van den Hout, W. Hop, O.P. van Diggelen, J.A.M. Smeitink, G.P.A. Smit, B.-T.T. Poll-The, H.D. Bakker, M.C.B. Loonen, J.B.C. de Klerk, A.J.J. Reuser and A.T. van der Ploeg, "The natural course of infantile Pompe's disease: 20 original cases compared with 133 cases from the literature", *Pediatrics* **112(2),** 332–340 (2003). https://doi.org/10.1542/peds.112.2.332
8. P.S. Kishnani and R.R. Howell, "Pompe disease in infants and children", *J. Pediatr.* **144(5 Suppl.),** S35–S43 (2004). https://doi.org/10.1016/j.jpeds.2004.01.053
9. P.S. Kishnani, R.D. Steiner, D. Bali, K. Berger, B.J. Byrne, L.E. Case, J.F. Crowley, S. Downs, R.R. Howell, R.M. Kravitz, J. Mackey, D. Marsden, A.M. Martins, D.S. Millington, M. Nicolino, G. O'Grady, M.C. Patterson, D.M. Rapoport, A. Slonim, C.T. Spencer, C.J. Tifft and M.S. Watson, "Pompe disease diagnosis and management guideline", *Genet. Med.* **8(5),** 267–288 (2006). https://doi.org/10.1097/01.gim.0000218152.87434.f3
10. B.J. Byrne, P.S. Kishnani, L.E. Case, L. Merlini, W. Müller-Felber, S. Prasad. A. van der Ploeg, "Pompe disease: Design, methodology, and early findings from the Pompe Registry". *Mol. Genet. Metab.* **103(1),** 1–11 (2011). https://doi.org/10.1016/j.ymgme.2011.02.004
11. P.S. Kishnani, M. Nicolino, T. Voit, R.C. Rogers, A.C.-H. Tsai, J. Waterson, G.E. Herman, A. Amalfitano, B.L. Thurberg, S. Richards, M. Davison, D. Corzo and Y.T. Chen, "Chinese hamster ovary cell-derived recombinant human acid alpha-glucosidase in infantile-onset Pompe disease", *J. Pediatr.* **149(1),** 89–97 (2006). https://doi.org/10.1016/j.jpeds.2006.02.035
12. P.S. Kishnani, D. Corzo, M. Nicolino, B. Byrne, H. Mandel, W.L. Hwu, N. Leslie, J. Levine, C. Spencer, M. McDonald, J. Li, J. Dumontier, M. Halberthal, Y.H. Chien, R. Hopkin, S. Vijayaraghavan, D. Gruskin, D. Bartholomew, A. van der Ploeg, J.P. Clancy, R. Parini, G. Morin, M. Beck, G.S. De la Gastine, M. Jokic, B. Thurberg, S. Richards, D. Bali, M. Davison, M.A. Worden, Y.T. Chen and J.E. Wraith, "Recombinant human acid α-glucosidase: major clinical benefits in infantile-onset Pompe disease", *Neurology* **68(2),** 99–109 (2007). https://doi.org/10.1212/01.wnl.0000251268.41188.04
13. M. Nicolino, B. Byrne, J.E. Wraith, N. Leslie, H. Mandel, D. Freyer, G. Arnold, E. Pivnick, C. Ottinger, P. Robinson, J. Loo, M. Smitka, P. Jardine, L. Tatò, B. Chabrol, S. McCandless, S. Kimura, L. Mehta, D. Bali, A. Skrinar, C. Morgan, L. Rangachari, D. Corzo and P. Kishnani, "Clinical outcomes after long-term treatment with alglucosidase alfa in infants and children with advanced Pompe disease", *Genet. Med.* **11(3),** 210–219 (2009). https://doi.org/10.1097/GIM.0b013e31819d0996
14. B.L. Thurberg, C.L. Maloney,C. Vaccaro, K. Afonso, A.C.-H. Tsai, E. Bossen, .S Kishnani and M. O'Callaghan, "Characterization of pre- and post-treatment pathology after enzyme replacement therapy for Pompe disease", *Lab. Investig.* **86,** 1208–1220 (2006). https://doi.org/10.1038/labinvest.3700484
15. S.N. Prater, T.T. Patel, A.F. Buckley, H. Mandel, E. Vlodavski, S.G. Banugaria, E.J. Feeney, N. Raben and P.S. Kishnani, "Skeletal muscle pathology of infantile Pompe disease during long-term enzyme replacement therapy", *Orphanet J. Rare Dis.* **8(1),** 90 (2013). https://doi.org/10.1186/1750-1172-8-90
16. P.S. Kishnani, D. Corzo, N.D. Leslie, D. Gruskin, A. Van der Ploeg, J.P. Clancy, R. Parini, G. Morin, M. Beck, M.S. Bauer, M. Jokic, C.-E. Tsai, B.W.H. Tsai, C. Morgan, T. O'Meara, S. Richards, E.C. Tsao and H. Mandel, "Early treatment with alglucosidase alpha prolongs long-term survival of infants with Pompe disease", *Pediatr. Res.* **66(3),** 329 (2009). https://doi.org/10.1203/PDR.0b013e3181b24e94

17. S.N. Prater, S.G. Banugaria, S.M. DeArmey, E.G. Botha, E.M. Stege, L.E. Case, H.N. Jones, C. Phornphutkul, R.Y. Wang, S.P. Young and P.S. Kishnani, "The emerging phenotype of long-term survivors with infantile Pompe disease", *Genet. Med.* **14(9),** 800 (2012). https://doi.org/10.1038/gim.2012.44

18. L.R. DeRuisseau, D.D. Fuller, K. Qiu, K.C. DeRuisseau, W.H. Donnelly Jr, C. Mah, P.J. Reier and B.J. Byrne, "Neural deficits contribute to respiratory insufficiency in Pompe disease", *Proc. Natl. Acad. Sci.* **106(23),** 9419–9424 (2009). https://doi.org/10.1073/pnas.0902534106

19. Y.-H. Chien, N.-C. Lee, S.-F. Peng and W.-L. Hwu, "Brain development in infantile-onset Pompe disease treated by enzyme replacement therapy", *Pediatr. Res.* **60(3),** 349 (2006). https://doi.org/10.1203/01.pdr.0000233014.84318.4e

20. T.A. Burrow, L.A. Bailey, D.G. Kinnett and R.J. Hopkin, "Acute progression of neuromuscular findings in infantile Pompe disease", *Pediatr. Neurol.* **42(6),** 455 (2010). https://doi.org/10.1016/j.pediatrneurol.2010.02.006

21. C.M. van Gelder, C.I. van Capelle, B.J. Ebbink, I. Moor-van Nugteren, J.M. van den Hout, M.M. Hakkesteegt, P.A. van Doorn, I.F. de Coo, A.J. Reuser, H.H. de Gier and A.T. van der Ploeg, "Facial-muscle weakness, speech disorders and dysphagia are common in patients with classic infantile Pompe disease treated with enzyme therapy", *J. Inherit. Metab. Dis.* **35(3),** 505 (2012). https://doi.org/10.1007/s10545-011-9404-7

22. P.S. Kishnani, P.C. Goldenberg, S.L. DeArmey, J. Heller, D. Benjamin, S. Young, D. Bali, S.A. Smith, J.S. Li, H. Mandel, D. Koeberl, A. Rosenberg and Y.T. Chen, "Cross-reactive immunologic material status affects treatment outcomes in Pompe disease infants", *Mol. Genet. Metab.* **99(1),** 26 (2010). https://doi.org/10.1016/j.ymgme.2009.08.003

23. L.E. Case, C. Bjartmar, C. Morgan, R. Casey, J. Charrow, J.P. Clancy, M. Dasouki, S. DeArmey, K. Nedd, M. Nevins, H. Peters, D. Phillips, Z. Spigelman, C. Tifft and P.S. Kishnani, "Safety and efficacy of alternative alglucosidase alfa regimens in Pompe disease", *Neuromuscul. Disord.* **25(4),** 321 (2015). https://doi.org/10.1016/j.nmd.2014.12.004

24. J. Hordeaux, L. Dubreil, J. Deniaud, F. Iacobelli, S. Moreau, M. Ledevin, C. Le Guiner, V. Blouin, J. Le Duff, A. Mendes-Madeira, F. Rolling, Y. Cherel, P. Moullier and M.A. Colle, "Efficient central nervous system AAVrh10-mediated intrathecal gene transfer in adult and neonate rats", *Gene Ther.* **22(4),** 316 (2015). https://doi.org/10.1038/gt.2014.121

25. K. Bey, C. Ciron, L. Dubreil, J. Deniaud, M. Ledevin, J. Cristini, V. Blouin, P. Aubourg and M.A. Colle, "Efficient CNS targeting in adult mice by intrathecal infusion of single-stranded AAV9-GFP for gene therapy of neurological disorders", *Gene Ther.* **24(5),** 325 (2017). https://doi.org/10.1038/gt.2017.18

26. J. Hordeaux, L. Dubreil, C. Robveille, J. Deniaud, Q. Pascal, B. Dequéant, J. Pailloux, L. Lagalice, M. Ledevin, C. Babarit, P. Costiou, F. Jamme, M. Fusellier, Y. Mallem, C. Ciron, C. Huchet, C. Caillaud and M.A. Colle, "Long-term neurologic and cardiac correction by intrathecal gene therapy in Pompe disease", *Acta Neuropathol. Commun.* **5(1),** 66 (2017). https://doi.org/10.1186/s40478-017-0464-2

27. Y.-T. Teng, W.-J. Su, J.-W. Hou and S.-F. Huang, "Infantile-onset glycogen storage disease type II (Pompe disease): report of a case with genetic diagnosis and pathological findings", *Chang Gung Med. J.* **27(5),** 379 (2004).

28. L.D. Hobson-Webb, A.D. Proia, B.L. Thurberg, S. Banugaria, S.N. Prater and P.S. Kishnani, "Autopsy findings in late-onset Pompe disease: a case report and systematic review of the literature", *Mol. Genet. Metab.* **106(4),** 462 (2012). https://doi.org/10.1016/j.ymgme.2012.05.007

29. A. van der Ploeg, P.G. Carlier, R.-Y. Carlier, J.T. Kissel, B. Schoser, S. Wenninger, A. Pestronk, R.J. Barohn, M.M. Dimachkie, O. Goker-Alpan, T. Mozaffar, L.D.M. Pena, Z. Simmons, V. Straub, M. Guglieri, P. Young, M. Boentert, P.-Y. Baudin, S. Wens, R. Shafi, C. Bjartmar and B.L. Thurberg, "Prospective exploratory muscle biopsy, imaging, and functional assessment in patients with late-onset Pompe disease treated with alglucosidase alfa: the embassy study", *Mol. Genet. Metab.* **119(1–2),** 115 (2016). https://doi.org/10.1016/j.ymgme.2016.05.013

30. E. Frezza, C. Terracciano, M. Giacanelli, E. Rastelli, G. Greco and R. Massa, "Late-onset Pompe disease with nemaline bodies", *Case Rep. Neurol. Med.* **2018,** 4127213 (2018). https://doi.org/10.1155/2018/4127213

31. L. Lagalice, J. Pichon, E. Gougeon, S. Soussi, J. Deniaud, M. Ledevin, V. Maurier, I. Leroux, S.

Durand, C. Ciron, F. Franzoso, L. Dubreil, T. Larcher, K. Rouger and M.-A. Colle, "Satellite cells fail to contribute to muscle repair but are functional in Pompe disease (glycogenosis type II)", *Acta Neuropathol. Commun.* **6(1),** 116 (2018). https://doi.org/10.1186/s40478-018-0609-y

32. L.M. Miller and P. Dumas, "Chemical imaging of biological tissue with synchrotron infrared light", *Biochim. Biophys. Acta Biomembr.* **1758(7),** 846 (2006). https://doi.org/10.1016/j.bbamem.2006.04.010

33. B.J. Zeskind, C.D. Jordan, W. Timp, L. Trapani, G. Waller, V. Horodincu, D.J. Ehrlich and P. Matsudaira, "Nucleic acid and protein mass mapping by live-cell deep-ultraviolet microscopy", *Nat. Methods* **4(7),** 567 (2007). https://doi.org/10.1038/nmeth1053

34. C. Chagnot, A. Vénien, F. Peyrin, F. Jamme, M. Réfrégiers, M. Desvaux and T. Astruc, "Deep UV excited muscle cell autofluorescence varies with the fibre type", *Analyst (Lond.)* **140(12),** 4189 (2015). https://doi.org/10.1039/C5AN00172B

35. F. Jamme, S. Kascakova, S. Villette, F. Allouche, S. Pallu, V. Rouam and M. Réfrégiers, "Deep UV autofluorescence microscopy for cell biology and tissue histology", *Biol. Cell* **105(7),** 277 (2013). https://doi.org/10.1111/boc.201200075

36. G.A. Wagnières, W.M. Star and B.C. Wilson, "*In vivo* fluorescence spectroscopy and imaging for oncological applications", *Photochem. Photobiol.* **68(5),** 603 (1998). https://doi.org/10.1111/j.1751-1097.1998.tb02521.x

37. M. Voicescu, M. Heinrich and P. Hellwig, "Steady-state and time resolved fluorescence analysis on tyrosine-histidine model compounds", *J. Fluoresc.* **19(2),** 257 (2009). https://doi.org/10.1007/s10895-008-0411-5

38. S. Pallu, G.Y. Rochefort, C. Jaffre, M. Refregiers, D.B. Maurel, D. Benaitreau, E. Lespessailles, F. Jamme, C. Chappard and C.-L. Benhamou, "Synchrotron ultraviolet microspectroscopy on rat cortical bone: involvement of tyrosine and tryptophan in the osteocyte and its environment", *PLoS One* **7(8),** e43930 (2012). https://doi.org/10.1371/journal.pone.0043930

39. J.-P. Echard, M. Thoury, B.H. Berrie, T. Séverin-Fabiani, A. Vichi, M. Didier, M. Réfrégiers and L. Bertrand, "Synchrotron DUV luminescence microimaging to identify and map historical organic coatings on wood", *Analyst (Lond.)* **140(15),** 5344 (2015). https://doi.org/10.1039/C5AN00483G

40. C. Chagnot, A. Vénien, F. Jamme, M. Réfrégiers, M. Desvaux and T. Astruc, "Hyperspectral deep ultraviolet autofluorescence of muscle fibers is affected by postmortem changes", *J. Agric. Food Chem.* **63(19),** 4782 (2015). https://doi.org/10.1021/acs.jafc.5b00668

41. F. Jamme, S. Villette, A. Giuliani, V. Rouam, F. Wien, B. Lagarde and M. Réfrégiers, "Synchrotron UV fluorescence microscopy uncovers new probes in cells and tissues", *Microsc. Microanal.* **16(5),** 507 (2010). https://doi.org/10.1017/S1431927610093852

42. F. Jamme, D. Bourquin, G. Tawil, A. Viksø-Nielsen, A. Buléon and M. Réfrégiers, "3D imaging of enzymes working *in situ*", *Anal. Chem.* **86(11),** 5265 (2014). https://doi.org/10.1021/ac403699h

43. A.D. Edelstein, M.A. Tsuchida, N. Amodaj, H. Pinkard, R.D. Vale and N. Stuurman, "Advanced methods of microscope control using μManager software", *J. Biol. Methods* **1(2),** 10 (2014). https://doi.org/10.14440/jbm.2014.36

44. A. Edelstein, N. Amodaj, K. Hoover, R. Vale and N. Stuurman, "Computer control of microscopes using μManager", *Curr. Protoc. Mol. Biol.* Ch. 14, Unit14.20 (2010). https://doi.org/10.1002/0471142727.mb1420s92

45. J. Schindelin, I. Arganda-Carreras, E. Frise, V. Kaynig, M. Longair, T. Pietzsch, S. Preibisch, C. Rueden, S. Saalfeld, B. Schmid, J.-Y. Tinevez, D.J. White, V. Hartenstein, K. Eliceiri, P. Tomancak and A. Cardona, "Fiji: an open-source platform for biological-image analysis", *Nat. Methods* **9(7),** 676 (2012). https://doi.org/10.1038/nmeth.2019

46. A. Gałat, "Study of the Raman scattering and infrared absorption spectra of branched polysaccharides", *Acta Biochim. Pol.* **27(2),** 135 (1980).

47. P. Heraud, S. Caine, N. Campanale, T. Karnezis, D. McNaughton, B.R. Wood, M.J. Tobin and C.C.A. Bernard, "Early detection of the chemical changes occurring during the induction and prevention of autoimmune-mediated demyelination detected by FT-IR imaging", *Neuroimage* **49(2),** 1180 (2010). https://doi.org/10.1016/j.neuroimage.2009.09.053

48. I. Dreissig, S. Machill, R. Salzer and C. Krafft, "Quantification of brain lipids by FTIR spectroscopy and partial least squares regression", *Spectrochim.*

Acta A Mol. Biomol. Spectrosc. **71(5),** 2069 (2009). https://doi.org/10.1016/j.saa.2008.08.008

49. F. Severcan and P.I. Haris, *Vibrational Spectroscopy in Diagnosis and Screening*. IOS Press (2010).

50. D.L. Wetzel, G.R. Post and R.A. Lodder, "Synchrotron infrared microspectroscopic analysis of collagens I, III, and elastin on the shoulders of human thin-cap fibroatheromas", *Vibr. Spectrosc.* **38,** 53–59 (2005). https://doi.org/10.1016/j.vibspec.2005.02.029

51. F. Palombo, S.G. Cremers, P.D. Weinberg and S.G. Kazarian, "Application of Fourier transform infrared spectroscopic imaging to the study of effects of age and dietary l-arginine on aortic lesion composition in cholesterol-fed rabbits", *J. R. Soc. Interface* **6(37),** 669 (2009). https://doi.org/10.1098/rsif.2008.0325

52. M.J. Hackett, J. Lee, F. El-Assaad, J.A. McQuillan, E.A. Carter, G.E. Grau, N.H. Hunt and P.A. Lay, "FTIR imaging of brain tissue reveals crystalline creatine deposits are an *ex vivo* marker of localized ischemia during murine cerebral malaria: general implications for disease neurochemistry", *ACS Chem. Neurosci.* **3(12),** 1017 (2012). https://doi.org/10.1021/cn300093g

53. W. André, C. Sandt, P. Dumas, P. Djian and G. Hoffner, "Structure of inclusions of Huntington's disease brain revealed by synchrotron infrared microspectroscopy: polymorphism and relevance to cytotoxicity", *Anal. Chem.* **85(7),** 3765 (2013). https://doi.org/10.1021/ac400038b

54. K. Araki, N. Yagi, Y. Ikemoto, H. Yagi, C.-J. Choong, H. Hayakawa, G. Beck, H. Sumi, H. Fujimura, T. Moriwaki, Y. Nagai, Y. Goto and H. Mochizuki, "Synchrotron FTIR micro-spectroscopy for structural analysis of Lewy bodies in the brain of Parkinson's disease patients", *Sci. Rep.* **5(1),** 17625 (2015). https://doi.org/10.1038/srep17625

55. A. Pascarella, C. Terracciano, O. Farina, L. Lombardi, T. Esposito, F. Napolitano, G. Franzese, G. Panella, F. Tuccillo, G. la Marca, S. Bernardini, S. Boffo, A. Giordano, G. Di Iorio, M.A.B. Melone and S. Sampaolo, "Vacuolated PAS-positive lymphocytes as an hallmark of Pompe disease and other myopathies related to impaired autophagy", *J. Cell. Physiol.* **233(8),** 5829 (2018). https://doi.org/10.1002/jcp.26365

56. F. Gatto, B. Rossi, A. Tarallo, E. Polishchuk, R. Polishchuk, A. Carrella, E. Nusco, F.G. Alvino, F. Iacobellis, E. De Leonibus, A. Auricchio, G. Diez-Roux, A. Ballabio and G. Parenti, "AAV-mediated transcription factor EB (TFEB) gene delivery ameliorates muscle pathology and function in the murine model of Pompe disease", *Sci. Rep.* **7(1),** 15089 (2017). https://doi.org/10.1038/s41598-017-15352-2

57. S.M.F. Turner, D.J. Falk, B.J. Byrne and D.D. Fuller, "Transcriptome assessment of the Pompe (GAA-/-) mouse spinal cord indicates widespread neuropathology", *Physiol. Genomics* **48(11),** 785 (2016). https://doi.org/10.1152/physiolgenomics.00075.2016

58. R. Drury, *Theory and Practice of Histological Techniques*, 6th Edn. Churchill Livingstone (1983).

59. G. Schaart, R.P. Hesselink, H.A. Keizer, G. van Kranenburg, M.R. Drost and M.K.C. Hesselink, "A modified PAS stain combined with immunofluorescence for quantitative analyses of glycogen in muscle sections", *Histochem. Cell Biol.* **122(2),** 161 (2004). https://doi.org/10.1007/s00418-004-0690-0

60. C. Sandt, J. Frederick and P. Dumas, "Profiling pluripotent stem cells and organelles using synchrotron radiation infrared microspectroscopy", *J. Biophotonics* **6(1),** 60 (2013). https://doi.org/10.1002/jbio.201200139

61. C. Peng, F. Chiappini, S. Kaščáková, M. Danulot, C. Sandt, D. Samuel, P. Dumas, C. Guettier and F. Le Naour, "Vibrational signatures to discriminate liver steatosis grades", *Analyst (Lond.)* **140(4),** 1107 (2015). https://doi.org/10.1039/C4AN01679C

62. C. Peng, S. Kaščáková, F. Chiappini, N. Olaya, C. Sandt, I. Yousef, D. Samuel, P. Dumas, C. Guettier and F. Le Naour, "Discrimination of cirrhotic nodules, dysplastic lesions and hepatocellular carcinoma by their vibrational signature", *J. Transl. Med.* **14(1),** 9 (2016). https://doi.org/10.1186/s12967-016-0763-6

63. N. Raben, K. Nagaraju, E. Lee, P. Kessler, B. Byrne, L. Lee, M. LaMarca, C. King, J. Ward, B. Sauer and P. Plotz, "Targeted disruption of the acid alpha-glucosidase gene in mice causes an illness with critical features of both infantile and adult human glycogen storage disease type II", *J. Biol. Chem.* **273(30),** 19086 (1998). https://doi.org/10.1074/jbc.273.30.19086

64. A. Barth, "Infrared spectroscopy of proteins", *Biochim. Biophys. Acta Bioenerg.* **1767(9),** 1073 (2007). https://doi.org/10.1016/j.bbabio.2007.06.004